Characteristics of $K_2Ca_2(SO_4)_3$:Eu TLD Nanophosphor for its Applications in Electron and Gamma rays Dosimetry

Nandkumar T. Mandlik[a*], P. D. Sahare[b*], Sachin R. Rondiya[c], Nelson Y. Dzade[c], A. V. Deore[d], S. S. Dahiwale[d], S. D. Dhole[d]

[a]Department of Physics, Fergusson College, Savitribai Phule Pune University, Pune 411004, Maharashtra, India.
[b]Department of Physics and Astrophysics, University of Delhi, Delhi 110007, India.
[c]School of Chemistry, Cardiff University, Main Building, Park Place, Cardiff, CF10 3AT, Wales, United Kingdom
[d]Department of Physics, Savitribai Phule Pune University, Pune 411007, Maharashtra, India.

[*]Corresponding author E-mail: nandkumar.mandlik@fergusson.edu, ntmandlik@gmail.com (NTM), pdsahare@physics.du.ac.in (PDS)

Abstract

Nanorods (~25 nm × 200 nm) of $K_2Ca_2(SO_4)_3$:Eu phosphor (powder) were synthesized by chemical coprecipitation method followed by annealing at 700 °C. Dimensions of nanorods were confirmed by TEM and XRD. The material (pellets) was irradiated by ^{60}Co gamma rays for various doses over the range of 0.1 Gy to 100 kGy and also by 6 MeV electrons at different fluences varying from 2.5×10^{11} e/cm^2 to 5×10^{13} e/cm^2 at room temperature. Thermoluminescence (TL) and photoluminescence (PL) of the gamma and electron irradiated phosphors were also studied. TL glow curve apparently exhibited a peak at around 152 °C with a small hump around 258 °C. The exact number of peaks in a glow curve were determined by thermal cleaning method and glow curves were further deconvoluted by CGCD method to determine trapping parameters. PL emission spectrum consisted of a single emission band at 388 nm (Eu^{2+} emission) on excitation by 320 nm. The intensity of this peak increased with the electron fluence up to 5×10^{12} e/cm^2 and decreases thereafter. The TL response is linear in the dose range from 0.1 Gy to 1 kGy of gamma radiation and electron fluence range from 2.5×10^{11} e/cm^2 to 2.5×10^{12} e/cm^2. The electronic structures of the pristine and Eu doped $K_2Ca_2(SO_4)_3$ materials were analyzed by means of first-principles density functional theory (DFT) calculations. The dosimetric characteristics suggest that the $K_2Ca_2(SO_4)_3$:Eu nanophosphor can be useful for its application in radiation dosimetry, especially, for measurement of high-doses of gamma and electrons.

1. Introduction

Thermoluminescence (TL) is a well-known technique widely used in the dose measurement of ionizing radiations such as UV, X-rays, gamma rays and swift heavy ion beams. The intensity of light emitted by phosphor is proportional to the irradiation doses given to it and by calibration with known doses of high-energy radiations; unknown doses could also be estimated. Thermoluminescence has applications in many fields such as personnel and environmental dosimetry, medical dosimetry, archaeological and geological dating, space dosimetry, etc. [1-3]. Nanophosphors are useful for the measurements of high doses of ionizing radiations, where microcrystalline thermoluminescence dosimetry (TLD) phosphors saturate [4-18]. Recently published reports describe some of the phosphors such as nanocrystalline $CaSO_4$:Dy, $K_2Ca_2(SO_4)_3$:Eu, LiF:Mg,Cu,P, $Ba_{0.97}Ca_{0.03}SO_4$:Eu, etc. and show that they are quite suitable for estimating very high doses for high-energy radiations like gamma rays, protons and swift heavy ions [4-18]. Researchers have been studying $K_2Ca_2(SO_4)_3$ microcrystalline phosphors since 1990 [19-23] and the doped/co-doped $K_2Ca_2(SO_4)_3$ nanophosphors since 2002 [4-6, 8, 12-16]. Alongside, efforts are also being made towards the development of $K_2Ca_2(SO_4)_3$:Eu based photoluminescent liquid crystal displays (PLLCD) [24]. All the reported phosphors were irradiated with gamma rays, ion beams and proton beam and their luminescence properties were studied. There, however, exist limited reports on the thermoluminescence (TL) characteristic of the nanophosphors with electron irradiation.

In this work, $K_2Ca_2(SO_4)_3$:Eu (0.1 mole %) nanophosphor has been prepared by chemical coprecipitation method. The irradiation was carried out using gamma rays and 6 MeV electron beam. The TL glow curves of the irradiated materials were recorded for a wide range of gamma doses, i.e., from 0.1 Gy to 100 kGy and wide range of electron fluences, i.e., from 2.5×10^{11} to 5×10^{13} e/cm^2. TL response curves of the gamma rays and electron beam irradiated materials were studied and explained in more details. The experimental TL glow curves are deconvoluted by using a Computerized Glow Curve Deconvolution (CGCD) software code [17, 18, 25] and their trapping parameters were determined. Before doing the deconvolution of the glow curves the exact peak positions (temperatures) and the number of glow peaks were confirmed by thermal cleaning method [17, 18, 26, 27]. The irradiated materials were also stored at room temperature, glow curves were recorded at different time intervals to study fading over a period of time. The minimum

detectable dose of $K_2Ca_2(SO_4)_3$:Eu nanophosphor was also determined. Moreover, the photoluminescence (PL) excitations and emissions spectra of unirradiated and electron beam irradiated nanomaterial were recorded at room temperature and studied.

2. Experimental Procedure

2.1. Method of Preparation

Nanorods of $K_2Ca_2(SO_4)_3$:Eu were prepared using the chemical reaction followed by Mandlik et al. [16, 18]. For this synthesis $CaCl_2$, KCl and $(NH_4)_2SO_4$ were used as the precursors and for Eu doping, 0.1 mol % $EuCl_2$ (AR grade) received from Sigma Aldrich was used. The precipitate obtained after the reaction was filtered and washed several times with distilled water. The cleaned powder was then dried at 120 °C in an oven for 12 h, annealed and quenched at 700 °C for 2 h in air [20]. The synthesized powder of 80 mg was mixed with 40 mg of Teflon powder (binder) and using a die, with 4-ton pressure for 3 minutes each time by a hydraulic press, circular pellets of approx. 1.0 mm thick and 10 mm diameter were made in the laboratory for recording TL. However, for taking PL studies the powder samples were used.

2.2. Irradiation with 6 MeV electrons and ^{60}Co gamma rays

The pellets of the $K_2Ca_2(SO_4)_3$:Eu nanorods were irradiated by 6 MeV electrons at different fluences, varying from 2.5×10^{11} to 5×10^{13} e/cm^2 at room temperature. The electron beam was made available from the Rack Track Microtron facility at the Department of Physics, Savitribai Phule Pune University [28]. Similarly, the pellets of the $K_2Ca_2(SO_4)_3$:Eu nanorods were also exposed by ^{60}Co gamma source available at Department of Chemistry, Savitribai Phule Pune University for various doses over the range 0.1 Gy to 100 kGy for comparison.

2.3. Characterization

XRD spectrum was recorded using Cu-target (Cu-Kα=1.54 Å) on Bruker AXS D8 Advance X ray Diffractometer. The elemental concentration of the sample was studied by energy-dispersive X-ray spectrometer (EDS) attached to the Scanning Electron Microscope (JEOL JSM-6360A). TEM images of the $K_2Ca_2(SO_4)_3$:Eu powder were obtained on the Transmission Electron

Microscope, "TECHNAI G2 20U-TWIN (FEI, Netherlands)," operated at 200 kV. TL glow curves were recorded using a computerized Nucleonix TLD Reader (Model TL1009I) by taking (~5.0 mg and 1.0 mm thick) pellet sample every time and heating it with a uniform rate of 5 °Cs^{-1} with the help of a temperature controller. In these measurements, at least three TL glow curves were recorded for each sample after desired radiation exposure to confirm the consistency in the measurements. Photoluminescence (PL) excitation and emission spectra were recorded using Perkin Elmer LS-55 Fluorescence Spectrophotometer (using xenon flash lamp as source and a wide band PMT as a detector). For taking PL, same amount (~200 mg) of powder sample was taken for every measurement.

2.4. Computational Details

The first-principles density functional theory (DFT) calculations are performed using the projected augmented wave (PAW) plane-wave basis, implemented in the Vienna Ab initio Simulation Package (VASP) [29-32]. The electronic exchange–correlation potential was calculated using the Perdew–Burke–Ernzerhof (PBE) generalized gradient approximation (GGA) functional [33, 34]. A plane-wave basis set with a kinetic energy cut off of 600 eV was employed to converge the total energy of the $CaSO_4$:Eu compound to within 10^{-6} eV. The atomic positions are optimized using a conjugate gradient scheme without any symmetric restrictions until the residual Hellman–Feynman forces on each atom converged to within 10^{-3} eV $Å^{-1}$. The Brillouin zone of $K_2Ca_2(SO_4)_3$ and $K_2Ca_2(SO_4)_3$:Eu are sampled using 5×5×5 mesh of Monkhorst-Pack *k*-points [35]. The $K_2Ca_2(SO_4)_3$ was modelled in the cubic crystal structure (space group $P2_13$, no:198) containing 76 atoms (8 K, 8 Ca, 12 S, and 48 O) and by substituting Eu atom at K or Ca sites resulted in the formation of $K_2Ca_2(SO_4)_3$:Eu. A higher k-points mesh of 7×7×7 was used to determine the electronic structures (band structure and partial density of states).

3. Results and discussions

3.1. Particle size

The XRD spectrum of the $K_2Ca_2(SO_4)_3$:Eu annealed at 700 °C is shown in Fig. 1. The recorded pattern exhibit diffraction peaks indicating $K_2Ca_2(SO_4)_3$:Eu is in the cubic phase with lattice constant, a = 10.32 Å which matches well with the same given in JCPDS Card No. 40-0545.

The average particle (grain) size of the nanorods was estimated from the line broadening of the XRD peaks using the Scherrer's formula [16]. The average grain size of the nanorods was found to be close to 32 nm, which confirm the nanocrystalline phase of the $K_2Ca_2(SO_4)_3$:Eu powder. The shape and size of these particles were also determined from the recorded TEM image shown in Fig. 2(a). This image shows that the particles are in the form of rods having diameter 20-30 nm and the length ~200 nm. It also highlights that they are of quite uniform shapes and sizes. The difference in the estimation of the particle size is within the experimental limits and may be due to the estimation by two different methods. The selected area electron diffraction (SAED) pattern shown in Fig. 2(b) identifies the crystalline nature of $K_2Ca_2(SO_4)_3$:Eu and confirms the cubic phase.

3.2. Energy Dispersive Spectroscopy (EDS)

The elemental composition of $K_2Ca_2(SO_4)_3$:Eu was obtained from the energy dispersive spectroscopy (EDS), which shown in Fig. 3. The EDS of the $K_2Ca_2(SO_4)_3$:Eu powder sample reveal that they are mainly composed of K, Ca, S and O with a small amount of Eu. The EDS pattern confirms the presence of Eu in the $K_2Ca_2(SO_4)_3$ powder and percentage of the impurity is very nearly equal to the doped value of Eu in $K_2Ca_2(SO_4)_3$. Table 1 lists the weight percentage as well as atomic percentage of the elements in the $K_2Ca_2(SO_4)_3$:Eu sample.

3.3. Thermoluminescence glow curves

The synthesized $K_2Ca_2(SO_4)_3$:Eu nanophosphor was used for estimation of the doses of 6 MeV electrons and ^{60}Co gamma rays. Fig. 4 shows the TL glow curves of $K_2Ca_2(SO_4)_3$:Eu nanophosphor exposed to gamma rays at different doses (0.1 Gy to 100 kGy) and Fig. 5 shows the TL glow curves after exposure to 6 MeV electrons at different fluences (from 2.5×10^{11} e/cm^2 to 5×10^{13} e/cm^2). The TL glow curves shown in Fig. 4 and Fig. 5 apparently show a single glow peak at 152 °C, and a small hump at 258 °C. As seen from Fig. 4 and Fig. 5, there is no significant change in the position of peak temperature; and the difference is within the experimental error of 3 °C; if the phosphor is irradiated for different gamma doses and electron fluences. These results indicate that the observed peaks in the glow curve of $K_2Ca_2(SO_4)_3$:Eu nanophosphor follow first-order kinetics [27, 36, 37]. It has also been observed that the nature of the TL glow curves does not change with the gamma dose and electron fluence. It is to be noted here that the above number

of glow peaks and the respective peak temperatures are as apparently seen in the respective glow curves. However, the exact number of peaks and their respective peak temperatures were confirmed by thermal cleaning method, further deconvoluted by CGCD method and are given in Section 3.4 (Figs. 7 and 8) along with their trapping parameters (Table 2).

3.4. Deconvolution of TL glow curves and calculation of trapping parameters

TL glow curves of $K_2Ca_2(SO_4)_3$:Eu nanophosphor exposed to different doses of γ-rays from ^{60}Co source (0.1 Gy to 100 kGy) and irradiated with different electron fluences (from 2.5×10^{11} e/cm^2 to 5×10^{13} e/cm^2) are shown in Figs. 4 and 5, respectively. It could be observed that there is no appreciable change in the peak temperatures of the respective dosimetry peaks (~152 °C) and also that of the other peaks in these glow curves. This shows that these peaks could follow first order kinetics [27, 36, 37]. Therefore, the Computerized Glow Curve Deconvolution (CGCD) method for curve fitting in both gamma and electron irradiated $K_2Ca_2(SO_4)_3$:Eu nanophosphor was done using the glow curve deconvolution (GCD) function (Eqn. 1), suggested by Kitis [38], for the first order kinetics glow curves. Before doing the deconvolution, the exact peak positions (temperatures) and the number of glow peaks were confirmed by thermal cleaning method where irradiated samples were heated with a linear rate (5 °Cs^{-1}) at the interval of 5 °C up to a certain point. The heating was abruptly stopped (T_{stop} point) by switching off the power to the heater. The sample was then cooled down and reheated to obtain a glow curve and the position (maximum peak temperature T_m) of the corresponding peak was noted. This procedure was repeated several times by re-irradiating the same sample each time and by increasing the T_{stop} temperature by 5 °C higher value than the earlier [17, 18, 26, 27]. The T_m vs. T_{stop} values were plotted to obtain a staircase type of curve where the T_m values corresponding to the stairs (horizontally flat portions of the curve) are the respective maximum peak temperatures. The plot of T_m vs. T_{stop} for $K_2Ca_2(SO_4)_3$:Eu nanophosphor irradiated for 1 kGy of gamma dose is shown in Fig. 6.

Glow curve deconvolution (GCD) function suggested by Kitis [38] for the first order:

$$I(T) = I_m exp\left[1 + \frac{E}{kT}\frac{T-T_m}{T_m} - \frac{T^2}{T_m^2} exp\left(\frac{E}{kT}\frac{T-T_m}{T_m}\right)\left(1 - \frac{2kT}{E}\right) - \frac{2kT_m}{E}\right] \qquad (1)$$

Here, *I (T)* is the TL intensity at temperature *T* (K), I_m is the maximum peak intensity, T_m is the temperature corresponding to maximum peak intensity I_m, *E*, trap depth or the thermal activation energy (eV) needed to free the trapped electrons and *k*, the Boltzmann's constant (8.6×10^{-5} eVK^{-1}).

The frequency factor *S* is obtained from the following equation for the first order:

$$S = \frac{\beta E}{kT_m^2} \exp\left(\frac{E}{kT_m}\right) \quad (2)$$

where, β is the linear heating rate.

A typical deconvoluted TL curves and the theoretical curve fitting with the experimental TL glow curves (after convolution) for $K_2Ca_2(SO_4)_3$:Eu nanophosphor irradiated with 10 kGy of γ-dose and 5×10^{13} e/cm^2 electron fluence are given in Figs. 7 and 8, respectively. The goodness of the fitting, i. e., figure of merit (FOM) for these fittings is found to be in the range 1.87% to 1.92% which is considered as good. This shows that experimental and theoretical glow curves are in good agreement and very much overlapping on each other. The deconvolution of the experimental curves has revealed some more hidden glow peaks and the presence of these peaks was confirmed by thermal cleaning (staircase of T_m–T_{stop} plot) as shown in Fig. 6.

The trap depths or activation energies (E) of the deconvoluted glow peaks were calculated using Chen's set of empirical formulae [39, 40] as follows:

$$E_\alpha = c_\alpha\left(\frac{kT_m{}^2}{\alpha}\right) - b_\alpha(2kT_m) \quad (3)$$

with

$\alpha = \tau,\ \delta,\ \omega,$

$\tau = T_m - T_1,\ \delta = T_2 - T_m, \omega = T_2 - T_1,$

$c_\tau = 1.51 + 3.0(\mu_g - 0.42),$

$c_\delta = 0.976 + 7.3(\mu_g - 0.42),$

$c_\omega = 2.52 + 10.2(\mu_g - 0.42)$,

$b_\tau = 1.58 + 4.2(\mu_g - 0.42)$,

$b_\delta = 0, \quad b_\omega = 1.$

To determine the order of kinetic, the form factor was calculated by using the equation,

$$\mu_g = \frac{T_2 - T_m}{T_2 - T_1} \tag{4}$$

μ_g was found to be ~0.42 for all the deconvoluted and theoretically fitted glow peaks. The calculated trapping parameters are summarized in Table 2.

The TL glow curves shown in Fig. 4 and Fig. 5 apparently shows a single glow peak at 152 °C, and a small hump at 258 °C. But after deconvolution it is observed that, the TL glow curves show four peaks at 149, 162, 206, 259 °C for gamma irradiated nanophosphor and at 150, 166, 204, 259 °C for electron irradiated nanophosphor, respectively. It could be observed from the activation energy values (Table 2) that there is existence of discrete deep and shallow trap levels spread over the range from 0.75 to 1.24 eV. In case of microcrystalline material there is less spread (narrow range) of trap levels [7, 9, 17, 18]. This could be attributed to the widening of the band gap due to decrease in particle size and its effect on the reorganization of the local energy levels of the impurity(ies) responsible for formation of traps levels accordingly in nanocrystalline materials [7, 9, 17]. It could be observed from the data of Table 2 that there is not much change in the trapping parameters (viz. peak temperatures, activation energies and frequency factors) of the gamma and electron irradiated materials. This is quite understandable from the fact that both kinds of radiations are not densely ionizing, the local energy levels of the impurity ions remain the same in both the cases and the traps are generated not only by the incident ionizing but the secondary radiations also.

3.5. TL Response curve

Fig. 9(a) shows the TL response plot (TL peak intensity vs dose) of the $K_2Ca_2(SO_4)_3$:Eu nanophosphor irradiated with ^{60}Co gamma rays. It is observed from the Fig. 9(a) that the TL peak intensity increases linearly with the dose of the gamma rays from 0.1 Gy to 1.0 kGy and then it saturates. The TL response plot (TL peak intensity vs electron fluence) of $K_2Ca_2(SO_4)_3$:Eu nanophosphor irradiated with 6 MeV electrons is shown in Fig. 9(b). It is linear over the fluence range from 2.5×10^{11} e/cm^2 to 2.5×10^{12} e/cm^2 and beyond 2.5×10^{12} e/cm^2 fluence, the saturation effect is observed. There is early saturation for electron irradiation compared to gamma radiation. The possible reason is that, in both the cases (gamma rays and electron beam irradiation) the radiations interacts with the materials (matter) and deposit energy directly as well as indirectly, i. e., it goes through majorly three process photoelectric effect, Compton effect and pair production (not possible here due to energy limitations). The secondary radiations generated (inside the host) via these processes then further deposit the energy in phosphor which is stored. However, the difference in saturation doses (1.0 kGy for gamma rays and 2.5×10^{12} e/cm^2 fluence corresponding to 775 Gy, determined using ESTAR code) may be attributed to the difference in their energies and/or the kinds of radiations (one is electromagnetic while the other one charged particles) [41].

Generally, microcrystalline phosphors show linearity up to 100 Gy dose and nanophosphors have extended linear dose response up to 10 kGy, depending upon the size of nanoparticles [7, 9, 12, 17, 18]. The linear behavior of TL response curve can be explained on the basis of Unified Interaction Model (UNIM) [42, 43] which was developed to simulate thermoluminescence linear/supralinear dose response and the dependence of the linearity on ionization-density. It has now been proved that the luminescent material consists of atomically localized trapping centers (TCs)/luminescence centers (LCs). At low doses, recombination occurs within the trapping centre and as the dose increases trapping centers are increasingly populated thereby leading to increased luminescent efficiency which gives rise a linear dose response. At very high doses, more and more tracks are produced which get overlapped on each other that may not give extra TL intensity and thus lead to saturation. In the case of nanophosphor, tiny size of particles missed at low doses, become targeted at high doses and now generate trapping centers (TCs)/luminescence centers (LCs) [12, 16]. The set of analyses confirmed that the nanophosphors show TL response over a wide range/higher doses.

When the radiation passing through the material some energy from the radiation is absorbed, used for ionization and stored inside in the form of traps. The length of the track is very short and limited to the size in case of nanoparticles. Some of the radiations might be missing the nanoparticles due its tiny size at low doses. Moreover, as mentioned earlier, the traps are generated not only by the incident radiation but also by the secondary radiations generated due to interactions. In case of microcrystalline particles on the other hand the track lengths would be much longer as they pass through a much larger volume. The tracks near the surface may also not yield TL as most of them may be nonradiative. Thus, the TL yield would be more for microcrystalline material than its nanoform. However, at high-doses more and more tracks would be formed generating a greater number of traps/LCs. Thus, the tracks would be more overlapping in microcrystalline particles. This would be leading to early saturation in case of microcrystalline TLD phosphors while in nanoparticles they would still be increasing giving rise to wider dose ranges than the microcrystalline particles/material. This has also been observed here as the saturation for $K_2Ca_2(SO_4)_3$:Eu nanophosphor could be seen at around 1.0 kGy.

For dosimetric purposes, a thermoluminescent phosphor is expected to show a relatively simple glow curve (no interfering glow peaks), dosimetric peak is at higher temperature (as it shows lesser fading), high TL sensitivity, long term stability of the stored information at room temperature (namely low fading); good linearity of the TL signal in the specific useful range of radiation dose. The present $K_2Ca_2(SO_4)_3$:Eu nanophosphor has a single glow peak at 152 °C and has negligible fading (around 10%) over the period of 2 months with no shielding from the ambient environmental conditions. It has high sensitivity compared to other nanophosphors and very linear response over a wide range of exposures, i.e. up to 1.0 kGy. Thus, considering above facts, the presented $K_2Ca_2(SO_4)_3$:Eu nanophosphor could find its application in radiation dosimetry for high dose measurements. This is important in food preservation and cancer therapy where high doses are required.

3.6. Correlation between electron fluence and gamma dose

The dose (D) in the material by the electron energy deposition is calculated using the formula,

$$D(Gy) = 1.602 \times 10^{-10} \times \frac{1}{\rho}\frac{dE}{dx}(MeVcm^2gm^{-1}) \times n \quad (1)$$

where, n is the particle fluence (cm^{-2}), ρ is the density of the irradiated material ($g\text{-}cm^{-3}$), and dE/dx is the main energy loss calculated using the ESTAR code [44]. The doses for different electron fluences are shown below in Table 3.

It is observed that, there will not be any change in the nature of the electron fluence/equivalent dose response curve as Eqn. 1 is a linear relation. The sensitivity of the material to the two different kinds of radiations cannot be compared qualitatively due to their different natures and interactions with the target material. Considering the fact, if these results are compared for both radiations, it is concluded that the material is more sensitive for 6 MeV electron beam than gamma rays. So, if it is more sensitive it would also saturate early. Along with the saturation behavior, the sensitivity of the material is also an important parameter for the measurements of low doses.

3.7. Fading

The $K_2Ca_2(SO_4)_3$:Eu nanophosphor was tested for its fading. Several pellets of the phosphor material having equal masses were irradiated to 100 Gy dose of γ-rays from ^{60}Co source, stored in dark at ambient condition and TL was taken after 1, 10, 25, 50 days after irradiation. Fig. 10 shows the fading curve of the $K_2Ca_2(SO_4)_3$:Eu nanophosphor. In Fig. 10 total area (normalized) under the TL curves was taken. The total observed fading was ~3% in 1 day, ~6% in 10 days, ~8% in 25 days, ~10% in 50 days. Similar fading results were observed for electron irradiated $K_2Ca_2(SO_4)_3$:Eu nanophosphor.

3.8. Minimum Detectable Dose

The minimum detectable dose of $K_2Ca_2(SO_4)_3$:Eu nanophosphor was determined. For the measurement of minimum detectable dose, background reading of 10 unirradiated samples (weighing 10 mg each) was taken to determine standard deviation (σ) of the background signal.

The 10 samples (weighing 10 mg each) of $K_2Ca_2(SO_4)_3$:Eu nanophosphor were exposed to 0.1 Gy of gamma dose. The mean TL output (counts) of 10 samples was determined. The minimum detectable dose (MDD) was calculated by using the formula

$$MDD = \frac{3\sigma \times Dose}{Counts}$$

The calculated minimum detectable dose for $K_2Ca_2(SO_4)_3$:Eu nanophosphor was found to be ~1.0 mGy.

3.9. Photoluminescence

PL excitation and emission spectra of the unirradiated $K_2Ca_2(SO_4)_3$:Eu nanorods are shown in Fig. 11. When the materials were excited by 320 nm, single emission bands are observed at 388 nm, which can be assigned to the transitions between the lowest band of the $4f^6 5d$ configuration and the ground state $^8S_{7/2}$ of the $4f^7$ configuration of Eu^{2+} ion. The excitation spectra of these samples at λ_{em}= 388 nm show two major bands at 320 and 271 nm [8]. These results are different from those of $K_2Ca_2(SO_4)_3$:Eu microcrystalline samples. The emission spectrum for the microcrystalline samples have a broadband at 436 nm; while the excitation spectrum shows a major single band at 320 nm as reported earlier by Dhopte *et. al.* [21]. The wide blue shift observed in the emission bands of the present nanomaterials (i.e., 436 → 388 nm) agrees with the general trend on decreasing the particle size to nanoscale, which normally shows widening in the band gap and shifting/splitting in the energy levels [45, 46]. The very tiny size of the $K_2Ca_2(SO_4)_3$:Eu nanorods [Fig. 2] is expected to reduce the crystal field affects, resulting in widening of the band gap of Eu^{2+}. Moreover, the appearance of a new excitation band at 271 nm might also be ascribed to the same reason.

Fig. 12(a) shows PL emission spectra of $K_2Ca_2(SO_4)_3$:Eu nanomaterial irradiated at different electron fluences from 2.5×10^{11} e/cm^2 to 5×10^{13} e/cm^2 at excitation wavelength of 320 nm. Fig. 12(b) shows PL peak intensity of $K_2Ca_2(SO_4)_3$:Eu nanomaterials as a function of electron beam fluence. The PL peak intensity goes on increasing with electron fluence up to the 5×10^{12} e/cm^2. This may be due the increase in the electron trapping centers with the electron fluence. Further the PL peak intensity decreases with increase in the electron fluence. This may be attributed to

irradiation-induced amorphization as a result of cascade quenching. Similar results on decreasing the PL intensity with increasing ions fluences were also observed by Nagabhushana *et. al.* [47]. They have attributed this effect to the induced amorphization due to the use of energetic ions for irradiation and to the restructuring of the surface chemical species because of the energy deposited through electronic loss during the process of swift heavy ion irradiation and, formation of ion induced defects leading to nonradiative recombination centers. Similar results were also observed by A. Choubey et.al. [48] where they have attributed the decrease in the PL intensity of emission peak after ion irradiation to higher concentration of defects that generates nonradiative states within the forbidden gap.

3.10. Electronic structures

The structure and electronic properties of the $K_2Ca_2(SO_4)_3$:Eu which dictates its luminescence properties were obtained from first-principles DFT calculations. The cubic crystal structure containing 76 atoms (8 K, 8 Ca, 12 S, and 48 O) was employed for the $K_2Ca_2(SO_4)_3$ material (Fig. 13a). By substituting Eu atom at either Ca (Eu@Ca-site, Fig. 13b) or K (Eu@K-site, Fig. 13c) sites resulted in the formation of $K_2Ca_2(SO_4)_3$:Eu. The fully optimized lattice *a* parameter of the pure cubic $K_2Ca_2(SO_4)_3$ is predicted at a = 10.545 Å, compared to 10.569 Å and 10.445 Å for Eu substitution at Ca and K sites, respectively. The results indicate that Eu substitution at Ca site induces small expansion in the lattice, whereas substitution are K site resulted in small contraction of the lattice. This is consistent with the larger ionic radius of Eu^{2+} (1.31 Å) than Ca^{2+} (1.14 Å) but smaller than K^+ (1.52 Å).

The electronic projected density of states of the pure and Eu-doped $K_2Ca_2(SO_4)_3$ are shown in Fig. 14 (a-c). The band gap of the pure $K_2Ca_2(SO_4)_3$ is predicted to be 5.17 eV. An analysis of the electronic structure of the pure $K_2Ca_2(SO_4)_3$ (Fig. 14a) reveal that the top of the valence band is mainly composed of O-*p* orbitals in $K_2Ca_2(SO_4)_3$ whereas the bottom of the conduction band is mainly composed of Ca-*d* orbitals. Therefore, the optical response at the bottom of conduction bands is mainly related to the O-*p* → Ca-*d* charge transfer. Compared to the pure $K_2Ca_2(SO_4)_3$, we observed a shift in the valence maximum to energy level close -5.0 eV for Eu substitution at Ca (Fig. 14b) or K (Fig. 14c) sites. It is also worth noting that in the $K_2Ca_2(SO_4)_3$:Eu materials, the Fermi level (E_F) shift closer to the bottom of the conduction band indicating the formation of n-

type insulators (with the added Eu impurities acting as donors, i. e., they give additional electrons to the system). The state donor states appear in the band gap near Fermi level of the $K_2Ca_2(SO_4)_3$:Eu, and they could act shallow trapping sites for excited electron from the valence band. Consistent with the introduced Eu *d* and *f* states near the conduction, emissions in the $K_2Ca_2(SO_4)_3$:Eu materials can be assigned to transitions between the lowest band of the Eu-4*f* and Eu-5*d* configuration. As the valence is remained composed mainly of O-*p* states Eu-doped $K_2Ca_2(SO_4)_3$:Eu material, the luminescence characteristics and the optical response and at the bottom of conduction bands can be attributed to O-*p*→Eu-*f*→Eu-*d*→Ca-*d* charge transfers. The energy separation of over 3.18 eV between the peaks of the Eu-4*f* orbitals and the Ca-3*d,* O-2p-orbitals is consistent with the experimentally observed emission wavelength of 388 nm. The corresponding band structures of the pure and Eu-doped $K_2Ca_2(SO_4)_3$are shown in Fig. 14 (d-f). An analysis of the band structure reveals that the pure $K_2Ca_2(SO_4)_3$ exhibits the characteristic of direct band transition at the Γ high-symmetry point of the Brillouin zone. The appearance donor states near the conduction are clearly evident.

6. CONCLUSION

In this work detailed studies on effect of irradiation of $K_2Ca_2(SO_4)_3$:Eu nanorods by gamma and electrons are carried out in order to understand the TL behavior of this phosphor in its nanostructure form at a very wide range of doses/fluences. Taken together, studies implicate that the studied nanomaterial systems show a very wide linear TL response curves to gamma and electrons, significantly superior to the corresponding microcrystalline materials. The TL glow curves are deconvoluted by CGCD method and trapping parameters are determined. It is observed that there is not much change in the trapping parameters of the gamma and electron irradiated materials. The exact peak positions and the number of glow peaks are confirmed by thermal cleaning method. The PL studies showed a wide blue shift of about 46 nm in the emission bands for the nanomaterials compared to micromaterials in addition to the appearance of a new excitation band at 271 nm. This change has been attributed to the extension of the band gap of Eu^{2+} dopant. First-principles analysis of the electronic structures of the pristine $K_2Ca_2(SO_4)_3$ and doped $K_2Ca_2(SO_4)_3$:Eu materials show that they are large band gap insulators. Eu substitution at Ca or K sites is demonstrated to result in the formation of n-type insulators in which the Eu donate additional electrons to the system. The luminescence behavior of $K_2Ca_2(SO_4)_3$:Eu phosphor can

be attributed to the charge transitions near the absorption edge from O-*p*→Ca-*d* orbitals in $K_2Ca_2(SO_4)_3$ and through O-*p*→Eu-*d*→Ca-*d* orbitals in $K_2Ca_2(SO_4)_3$:Eu. Therefore, $K_2Ca_2(SO_4)_3$:Eu nanophosphor is useful for measurement of high-doses of gamma and electrons. Especially, for certain high dose irradiation applications, such as, food preservation. $K_2Ca_2(SO_4)_3$:Eu nanophosphor might be employed as an effective TL detector for gamma and electron irradiation.

Acknowledgements

SRR and NYD acknowledge the UK Engineering and Physical Sciences Research Council (EPSRC) for funding (Grant No. EP/S001395/1). This work has also used the computational facilities of the Advanced Research Computing at Cardiff (ARCCA) Division, Cardiff University, and HPC Wales. This work also made use of the facilities of ARCHER (http://www.archer.ac.uk), the UK's national supercomputing service via the membership of the UK's HEC Materials Chemistry Consortium, which is funded by EPSRC (EP/L000202). PDS would also like to thank Inter-University Accelerator Centre, New Delhi, India for partial financial assistance through the BTR-3 research project code No. UFR-64325.

References:

[1] S. W. S. McKeever, Thermoluminescence of Solids, Cambridge University Press (1985). https://doi.org/10.1017/CBO9780511564994

[2] S. W. S. McKeever, M. Moscovitch, P. D. Townsend, Thermoluminescence Dosimetry Materials: Properties and Uses, Nuclear Technology Publishing, Ashford, UK, (1995). ISBN:1870965191 9781870965194

[3] V. Kortov, Materials for thermoluminescent dosimetry: Current status and future trends, Radiat. Meas. 42(4-5) (2007) 576-581. https://doi.org/10.1016/j.radmeas.2007.02.067

[4] A. Pandey, R. G. Sonkawade, P. D. Sahare, Thermoluminescence and photoluminescence characteristics of nanocrystalline $K_2Ca_2(SO_4)_3$:Eu, J. Phys. D: Appl. Phys. 35(21) (2002) 2744–2747. https://doi.org/10.1088/0022-3727/35/21/309

[5] N. Salah, S. P. Lochab, P. D. Sahare, Effect of Tb^{3+} Co-Doping and Particle Size on $K_2Ca_2(SO_4)_3$:Eu Phosphor, Radiat. Eff. Defect Solids. 158 (2003) 819–825. DOI: 10.1080/10420150310001618232

[6] N. Salah, P. D. Sahare, S. Nawaz, S. P. Lochab, Luminescence Characteristics of $K_2Ca_2(SO_4)_3$:Eu,Tb Micro- and Nanocrystalline Phosphor, Radiat. Eff. Defect Solids 159 (2004) 321–334. DOI: 10.1080/10420150310001633648

[7] N. Salah, P. D. Sahare, S. P. Lochab, P. Kumar, TL and PL studies on $CaSO_4$:Dy nanoparticles, Radiat. Meas. 41 (2006) 40-47. doi:10.1016/j.radmeas.2005.07.026

[8] N. Salah, S. P. Lochab, D. Kanjilal, R. Ranjan, S. S. Habib, A. A. Rupasov, V. E. Aleynikov, Nanoparticles of $K_2Ca_2(SO_4)_3$:Eu as effective detectors for swift heavy ions, J. of Appl. Phy. 102 (2007) 064904, (1-8). DOI: 10.1063/1.2779237

[9] N. Salah, P. D. Sahare, A. A. Rupasov, Thermoluminescence of nanocrystalline LiF:Mg, Cu, P, J. Lumin. 124 **(**2007) 357–364. doi:10.1016/j.jlumin.2006.04.004

[10] S. P. Lochab, P. D. Sahare, R. S. Chauhan, N. Salah, R. Ranjan, A. Pandey, Thermoluminescence and photoluminescence study of nanocrystalline $Ba_{0.97}Ca_{0.03}SO_4$:Eu, J. Phys. D: Appl. Phys. 40(5) (2007) 1343–1350. https://doi.org/10.1088/0022-3727/40/5/006

[11] S. P. Lochab, D. Kanjilal, N. Salah, S. S. Habib, J. Lochab, R. Ranjan, E. Aleynikov, A. A. Rupasov, A. Pandey, Nanocrystalline $Ba_{0.97}Ca_{0.03}SO_4$:Eu for ion beam Dosimetry, J. Appl. Phys. 104 (2008) 033520, (1-4). https://doi.org/10.1063/1.2955459

[12] A. Pandey , S. Bahl, K. Sharma , R. Ranjan, P. Kumar , S. P. Lochab , V. E. Aleynikov, A. G. Molokanov, Thermoluminescence properties of nanocrystalline $K_2Ca_2(SO_4)_3$:Eu

irradiated with gamma rays and proton beam, Nucl. Instrum. Method. Phys. Res. B 269(3) (2011) 216-222. https://doi.org/10.1016/j.nimb.2010.12.005

[13] P. D. Sahare, J. S. Bakare, S. D. Dhole, P. Kumar, Effect of phase transition and particle size on thermoluminescence characteristics of nanocrystalline $K_2Ca_2(SO_4)_3:Cu^+$ phosphor, Radiat. Meas. 47 (2012) 1083-1091. http://dx.doi.org/10.1016/j.radmeas.2012.10.003

[14] Nandkumar Mandlik, V. N. Bhoraskar, B. J. Patil, S. S. Dahiwale, P. D. Sahare, S. D. Dhole, Thermoluminescence and photoluminescence properties of $K_2Ca_2(SO_4)_3$:Cu nanophosphor for gamma radiation dosimetry, Indian J. of Pure and Appl. Phy. 50 (2012) 859-862. http://nopr.niscair.res.in/handle/123456789/14923

[15] Nandkumar Mandlik, P. D. Sahare, B. J. Patil, V. N. Bhoraskar, S. D. Dhole, Thermoluminescence study of $K_2Ca_2(SO_4)_3$:Cu nanophosphor for gamma ray dosimetry, Nucl. Instrum. Method. Phys. Res. B 315 (2013) 273–277. http://dx.doi.org/10.1016/j.nimb.2013.05.073

[16] Nandkumar Mandlik, P. D.Sahare, M. S.Kulkarni, B. C.Bhatt, V. N. Bhoraskar, S. D. Dhole, Study of TL and optically stimulated luminescence of $K_2Ca_2(SO_4)_3$:Cu nanophosphor for radiation dosimetry, J. Lumin. 146 (2014) 128–132. http://dx.doi.org/10.1016/j.jlumin.2013.09.061

[17] Nandkumar Mandlik, S. D. Dhole, P. D. Sahare, J. S. Bakare, A. Balraj, B. C. Bhatt, Thermoluminescence studies of $CaSO_4$:Dy nanophosphor for application in high dose measurements, App. Radiat. Isotop. 148 (2019) 253–261. https://doi.org/10.1016/j.apradiso.2019.03.015

[18] N. T. Mandlik, P. D. Sahare, S. D. Dhole, A. Balraj, Effect of annealing temperature and phase change on thermoluminescence and photoluminescence of $K_2Ca_2(SO_4)_3$:Eu nanophosphor, Nucl. Instrum. Methods Phys. Res. B. (in Press). https://doi.org/10.1016/j.nimb.2020.07.011

[19] P. D. Sahare, S. V. Moharil, B. D. Bhasin, $K_2Ca_2(SO_4)_3$ for thermoluminescence dosimetry of a high-temperature environment, J. Phys. D: Appl. Phys. 22 (1989) 971-974. https://doi.org/10.1088/0022-3727/22/7/015

[20] P. D. Sahare, S. V. Moharil, A new high-sensitivity phosphor for thermoluminescence dosimetry, J. Phys. D: Appl. Phys. 23 (1990) 567-570. https://doi.org/10.1088/0022-3727/23/5/015

[21] S. M. Dhopte, P. L. Muthal, V. K. Kondawar, S. V. Moharil, P. D. Sahare, Characterization of $K_2Ca_2(SO_4)_3$:Eu phosphor, J. Phys. D: Appl. Phys. 24 (1991) 1869-1876. https://doi.org/10.1088/0022-3727/24/10/024

[22] A. Pandey, V. K. Sharma, D. Mohan, R. K. Kale, P. D. Sahare, Thermoluminescence characteristics of $K_2Ca_2(SO_4)_3$ doped with rare earths Eu and Dy. J. Phys. D: Appl. Phys. 35 (2002) 1330–1333. https://doi.org/10.1088/0022-3727/35/12/308

[23] P. D. Sahare, N. Salah, S. P. Lochab, T. Mohanty, D. Kanjilal, Modifications in TL characteristics of $K_2Ca_2(SO_4)_3$:Eu by ^{7}Li MeV ion beam, J. Phys. D: Appl. Phys. 38 (2005) 3995–4002. https://doi.org/10.1088/0022-3727/38/21/026

[24] A. Vecht A. C. Newport P. A. Bayley W. A. Crossland, Narrow band 390 nm emitting phosphors for photoluminescent liquid crystal displays, J. Appl. Phys. 84 (1998) 3827-3829. https://doi.org/10.1063/1.368561

[25] V. Pagonis, G. Kitis, C. Furetta, Numerical and Practical Exercises in Thermoluminescence, Springer Science Business Media, Inc, 2006. ISBN-10: 0-387-26063-3

[26] S. W. S. McKeever, On the Analysis of Complex Thermoluminescence Glow-Curves: Resolution into Individual Peaks, phys. stat. sol. (a) 62 (1980) 331-340. https://doi.org/10.1002/pssa.2210620139

[27] J. M. Kalita, M. L. Chithambo, Thermoluminescence of Al_2O_3:C,Mg: Kinetic analysis of the main glow peak, J. Lumin. 182 (2017) 177–182. http://dx.doi.org/10.1016/j.jlumin.2016.10.031

[28] V. B. Asgekar, R. K. Bhalla, B. S. Raye, M. R. Bhiday, V. N. Bhoraskar, Single-cavity 8 MeV race-track microtron, Pramana 15(5) (1980)479–493. https://www.ias.ac.in/article/fulltext/pram/015/05/0479-0493

[29] G. Kresse, D. Joubert, From ultrasoft pseudopotentials to the projector augmented-wave method, Phys. Rev. B: Condens. Matter Mater. Phys. 59(3) (1999) 1758-1775. https://doi.org/10.1103/PhysRevB.59.1758

[30] G. Kresse, J. Furthmüller, Efficiency of ab-initio total energy calculations for metals and semiconductors using a plane-wave basis set**,** Comput. Mater. Sci. 6(1) (1996) 15-50. https://doi.org/10.1016/0927-0256(96)00008-0

[31] G. Kresse, J. Hafner, *Ab initio* molecular dynamics for liquid metals, Phys. Rev. B: Condens. Matter Mater. Phys. 47 (1993) 558–561. https://doi.org/10.1103/PhysRevB.47.558

[32] P. E. Blöchl, Projector augmented-wave method, Phys. Rev. B: Condens. Matter Mater. Phys. 50 (1994) 17953-17979. https://doi.org/10.1103/PhysRevB.50.17953

[33] J. P. Perdew, K. Burke, M. Ernzerhof, Generalized Gradient Approximation Made Simple, Phys. Rev. Lett., 78 (1997) 1396. https://doi.org/10.1103/PhysRevLett.78.1396

[34] J. P. Perdew, K. Burke, M. Ernzerhof, Generalized Gradient Approximation Made Simple, Phys. Rev. Lett. 77 (1996) 3865–3868. https://doi.org/10.1103/PhysRevLett.77.3865

[35] H. J. Monkhorst, J. D. Pack, Special points for Brillonin-zone integrations, Phys. Rev. B: Condens. Matter Mater. Phys. 13 (1976) 5188-5192. https://doi.org/10.1103/PhysRevB.13.5188

[36] A. J. J. Bos, Theory of thermoluminescence, Radiat. Meas. 41 (2007) S45–S56. doi:10.1016/j.radmeas.2007.01.003

[37] M. S. Rasheedy, A. M. A. Amry, On the frequency factor obtained in case of thermoluminescence second order kinetics, J. Lumin. 63(3) (1995) 149–154. https://doi.org/10.1016/0022-2313(94)00047-G

[38] G. Kitis, J. M. Gomez-Ros, J. W. N. Tuyn, Thermoluminescence glow-curve deconvolution functions for first, second and general orders of kinetics, J. Phys. D: Appl. Phys. 31 (19) (1998) 2636-2641. https://doi.org/10.1088/0022-3727/31/19/037

[39] R. Chen, Glow Curves with General Order Kinetics, J. Electrochem. Soc. 116(9) (1969) 1254-1257. https://doi.org/10.1149/1.2412291

[40] R. Chen, Y. Kirsh, Analysis of Thermally Stimulated Processes, 1st ed., Pergamon Press, New York, (1981) pp. 162-164. https://doi.org/10.1149/1.2412291

[41] G. Shani, Radiation Dosimetry: Instrumentation and Methods, 2nd ed., CRC Press, New York, USA (2001), pp. 6-8. https://doi.org/10.1201/9780203710708

[42] S. Mahajna, Y. S. Horowitz, The unified interaction model applied to the gamma ray induced supralinearity and sensitization of peak 5 in LiF:Mg,Ti (TLD-100)**,** J. Phys. D: Appl. Phys. 30 (1997) 2603–2619. https://doi.org/10.1088/0022-3727/30/18/016

[43] Y. S. Horowitz, Theory of thermoluminescence gamma dose response: The unified interaction model, Nucl. Instrum. Method. Phys. Res. B 184(1-2) (2001) 68-84. https://doi.org/10.1016/S0168-583X(01)00712-1

[44] M. J. Berger, J. S. Coursey, M. A. Zucker, J. Chang (2005), ESTAR, PSTAR, and ASTAR: Computer Programs for Calculating Stopping-Power and Range Tables for Electrons, Protons, and Helium Ions (version 1.2.3). Available (Online) at https://physics.nist.gov/cgi-bin/Star/e_table-u.pl, National Institute of Standards and Technology, Gaithersburg, MD.

[45] P. Moriarty, Nanostructured materials, Rep. Prog. Phys. 64(3) (2001) 297- 381. https://doi.org/10.1088/0034-4885/64/3/201

[46] C. Xu, Q. Xue, Y. Zhong, Y. Cui, L. Ba, B. Zhao, N. Gu, Photoluminescent blue-shift of organic molecules in nanometre pores, Nanotechnology 13(1) (2002) 47-50. https://doi.org/10.1088/0957-4484/13/1/310

[47] H. Nagabhushana, B. N. Lakshminarasappa, F. Singh, D. K. Avasthi, Photoluminescence studies in swift heavy ion bombarded mullite, Nucl. Instrum. Methods Phys. Res. B 211(4) (2003) 545-548. https://doi.org/10.1016/S0168-583X(03)01709-9

[48] A. Choubey, S. K. Sharma , S. P. Lochabb, T. Shripathi, Effect of ion irradiation on optoelectronic properties of $Ba_{0.12}Sr_{0.88}SO_4$: Eu phosphor, Physica B 406(23) (2011) 4483–4488. https://doi.org/10.1016/j.physb.2011.09.012

Figure Captions:

Fig. 1. X-ray diffraction spectra of nanocrytstalline $K_2Ca_2(SO_4)_3$: Eu.

Fig. 2. (a) TEM image and **(b)** SAED pattern of $K_2Ca_2(SO_4)_3$: Eu nanorods.

Fig. 3. A typical EDS pattern of the $K_2Ca_2(SO_4)_3$:Eu nanophosphor.

Fig. 4. TL glow curves of $K_2Ca_2(SO_4)_3$:Eu nanophosphor exposed to different doses of ^{60}Co gamma source. The ordinate is to be multiplied by the numbers at the curves to get the relative intensities.

Fig. 5. TL glow curves of $K_2Ca_2(SO_4)_3$:Eu nanophosphor irradiated by 6 MeV electrons at different fluences. The ordinate is to be multiplied by the numbers at the curves to get the relative intensities.

Fig. 6. A typical T_m–T_{stop} plot for the $K_2Ca_2(SO_4)_3$:Eu nanophosphor exposed to 1 kGy of gamma dose from ^{60}Co source. In the staircase kind of curve the T_m corresponding to the stairs (horizontally flat portions of the curve) are the respective maximum peak temperatures.

Fig. 7. Comparison between the experimental (--o--) and the theoretically (—) fitted TL glow curves of $K_2Ca_2(SO_4)_3$:Eu nanophosphor exposed to 10 kGy of gamma dose from ^{60}Co source. Deconvoluted glow curves **a**, **b, c** and **d** are also shown.

Fig. 8. Comparison between the experimental (--o--) and the theoretically (—) fitted TL glow curves of $K_2Ca_2(SO_4)_3$:Eu nanophosphor irradiated with 5×10^{13} e/cm^2 electron fluence of 6 MeV electron beam from the Rack Track Microtron. Deconvoluted glow curves **a**, **b, c** and **d** are also shown.

Fig. 9. TL Response curve of $K_2Ca_2(SO_4)_3$:Eu nanophosphor exposed to **(a)** different doses of ^{60}Co gamma source, and **(b)** different fluences of electron irradiation.

Fig. 10. Fading curve of the $K_2Ca_2(SO_4)_3$:Eu nanophosphor.

Fig. 11. Photoluminescence excitation and emission spectra of unirradiated $K_2Ca_2(SO_4)_3$:Eu nanophosphor sample.

Fig. 12. (a) Photoluminescence emission spectra of electron irradiated $K_2Ca_2(SO_4)_3$:Eu nanocrystalline sample at excitation 320 nm and **(b)** PL intensity of 6 MeV electron beam irradiated $K_2Ca_2(SO_4)_3$:Eu nanophosphor as a function of electron beam fluence.

Fig. 13. The optimized structures (a) pure $K_2Ca_2(SO_4)_3$, (b) Eu substitution at Ca site (Eu@Ca-site), and (c) Eu substitution at K site (Eu@K-site). Colour code: K=purple; Ca=cyan; S=yellow; O=red, and Eu=green.

Fig. 14. The projected density of states of (a) pure $K_2Ca_2(SO_4)_3$, (b) Eu substitution at Ca site (Eu@Ca-site), and (c) Eu substitution at K site (Eu@K-site). The corresponding calculated band structure are shown in (d-f).

Fig. 1.

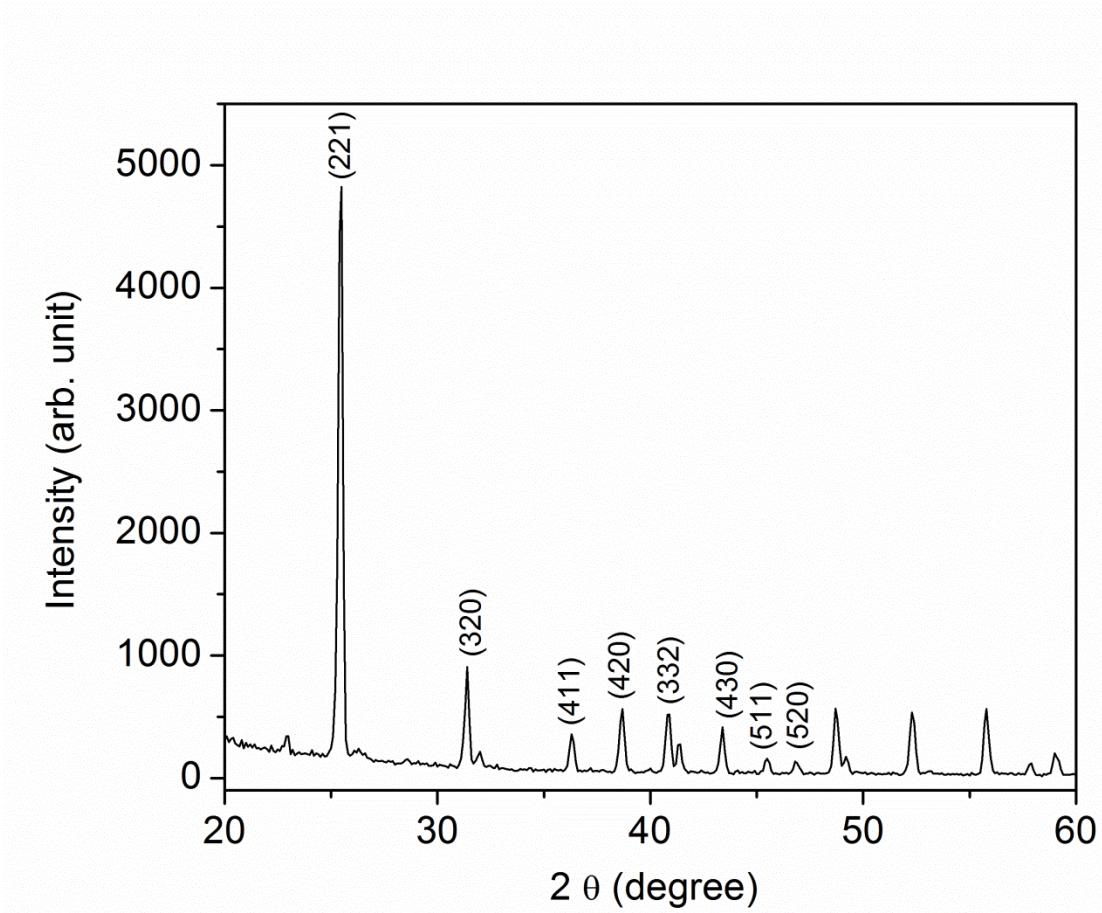
Intensity (arb. unit)
5000
4000
3000
2000
1000
0
20
30
40
50
60
2 θ (degree)
(221)
(320)
(411)
(420)
(332)
(430)
(511)
(520)

Fig. 2.

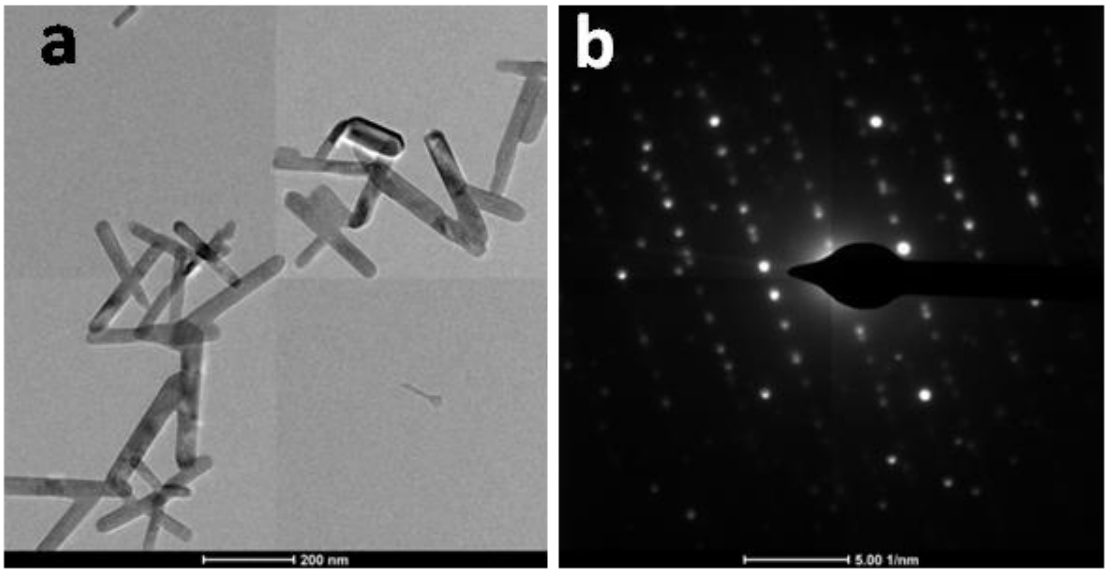

Fig. 3.

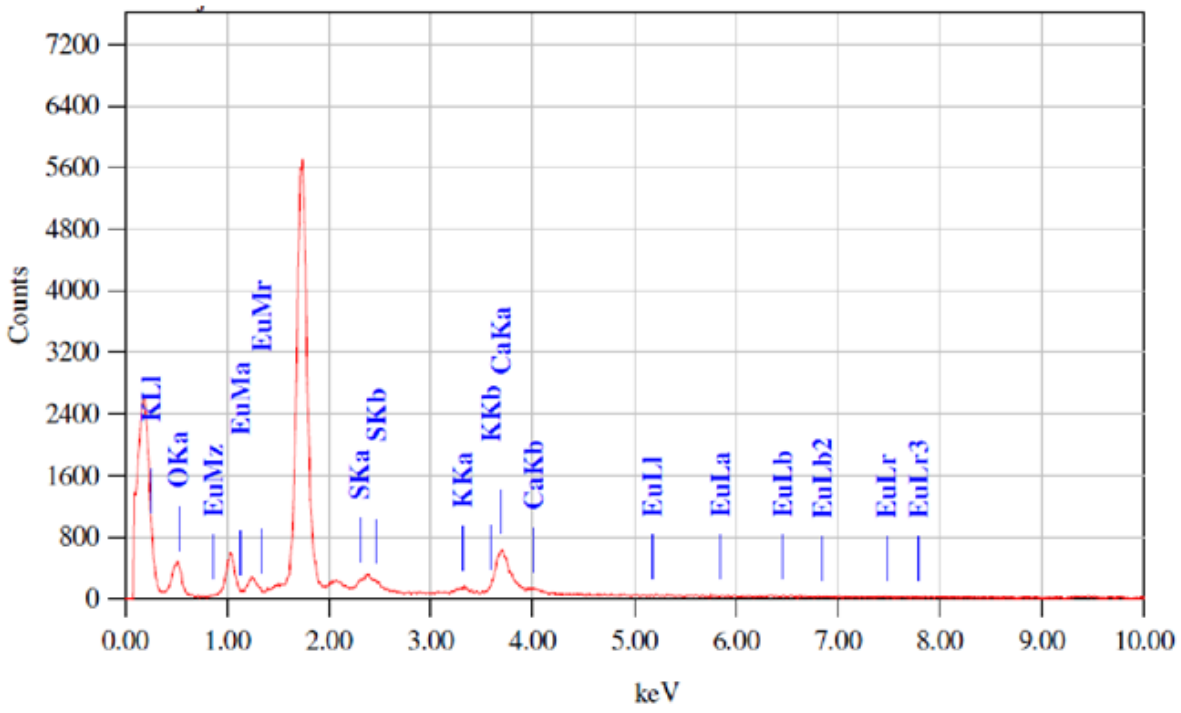
Counts
7200
6400
5600
4800
4000
3200
2400
1600
800
0
0.00
1.00
2.00
3.00
4.00
5.00
6.00
7.00
8.00
9.00
10.00
keV
KLl
OKa
EuMz
EuMa
EuMr
SKa
SKb
KKa
KKb
CaKa
CaKb
EuLl
EuLa
EuLb
EuLb2
EuLr
EuLr3

Fig. 4.

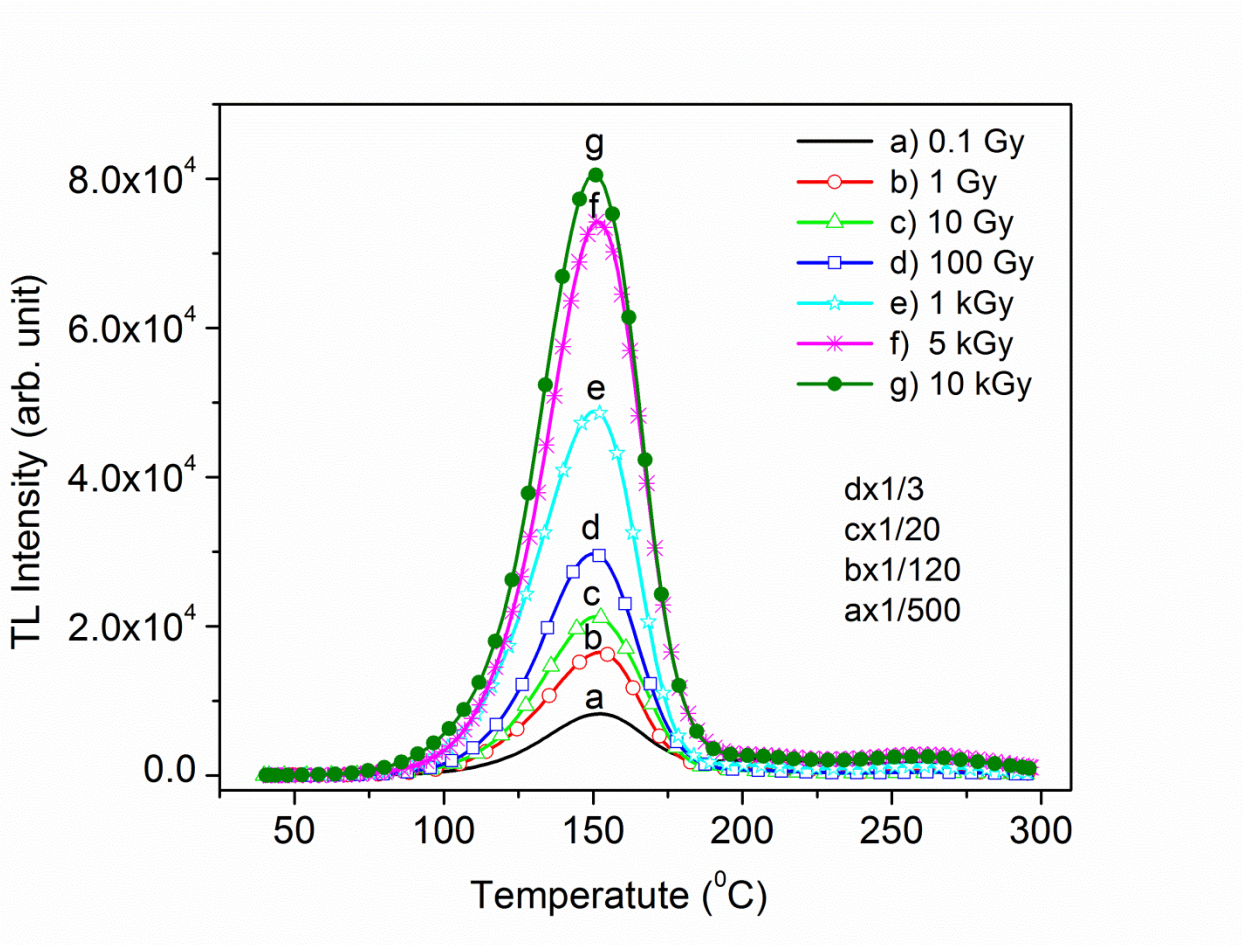
TL Intensity (arb. unit)
8.0x10^4
6.0x10^4
4.0x10^4
2.0x10^4
0.0
50
100
150
200
250
300
Temperatute (^0C)
a) 0.1 Gy
b) 1 Gy
c) 10 Gy
d) 100 Gy
e) 1 kGy
f) 5 kGy
g) 10 kGy
dx1/3
cx1/20
bx1/120
ax1/500
a
b
c
d
e
f
g

Fig. 5.

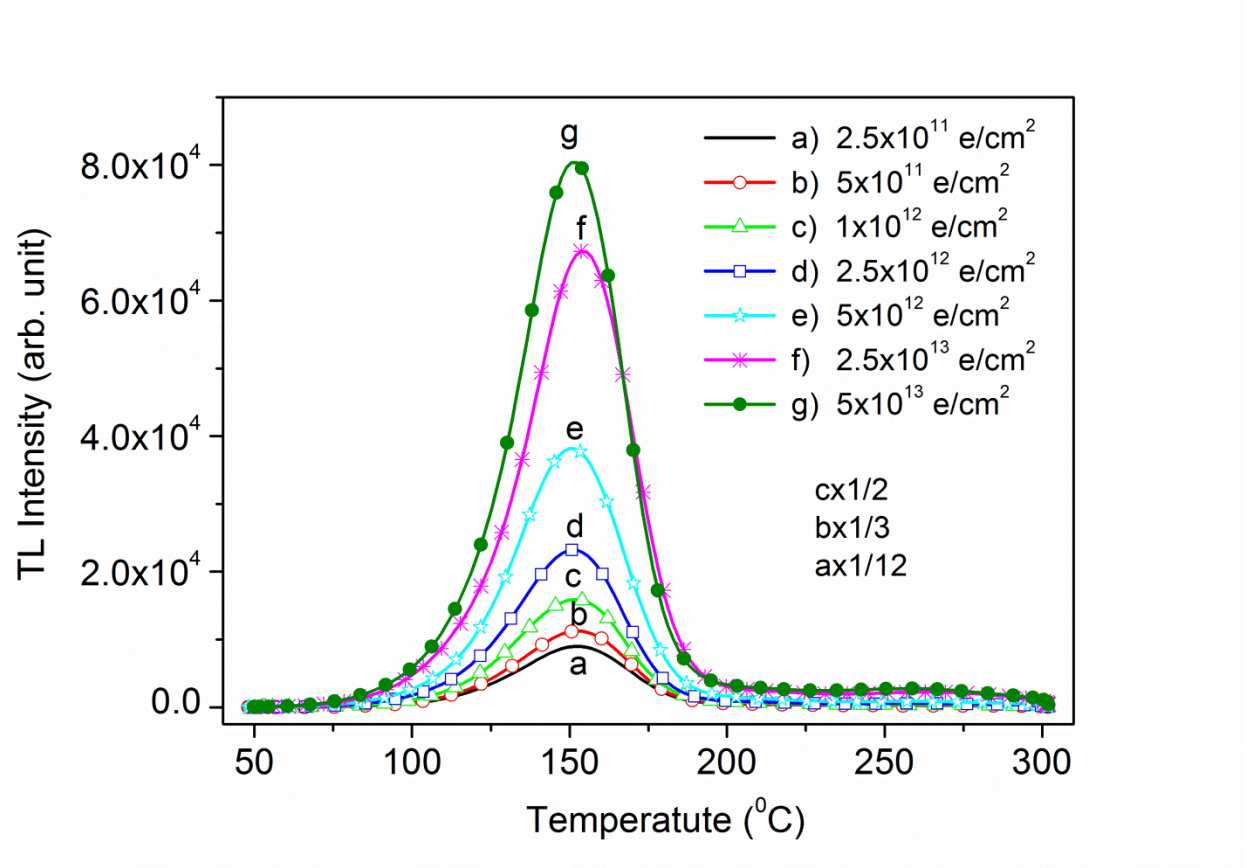
TL Intensity (arb. unit)
8.0x10^4
6.0x10^4
4.0x10^4
2.0x10^4
0.0
50
100
150
200
250
300
Temperatute (^0C)
a) 2.5x10^11 e/cm^2
b) 5x10^11 e/cm^2
c) 1x10^12 e/cm^2
d) 2.5x10^12 e/cm^2
e) 5x10^12 e/cm^2
f) 2.5x10^13 e/cm^2
g) 5x10^13 e/cm^2
cx1/2
bx1/3
ax1/12
a
b
c
d
e
f
g

Fig. 6.

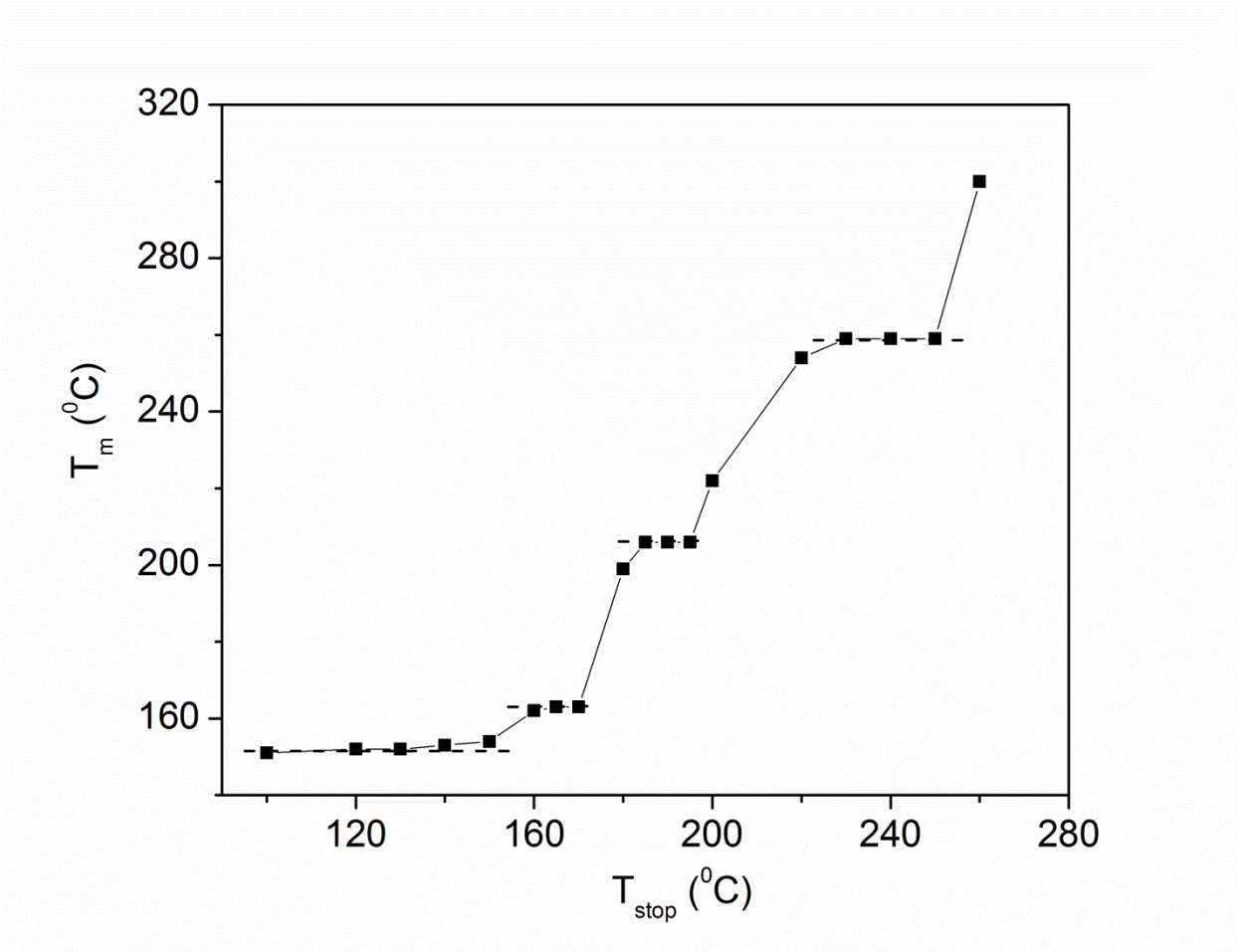

Fig. 7.

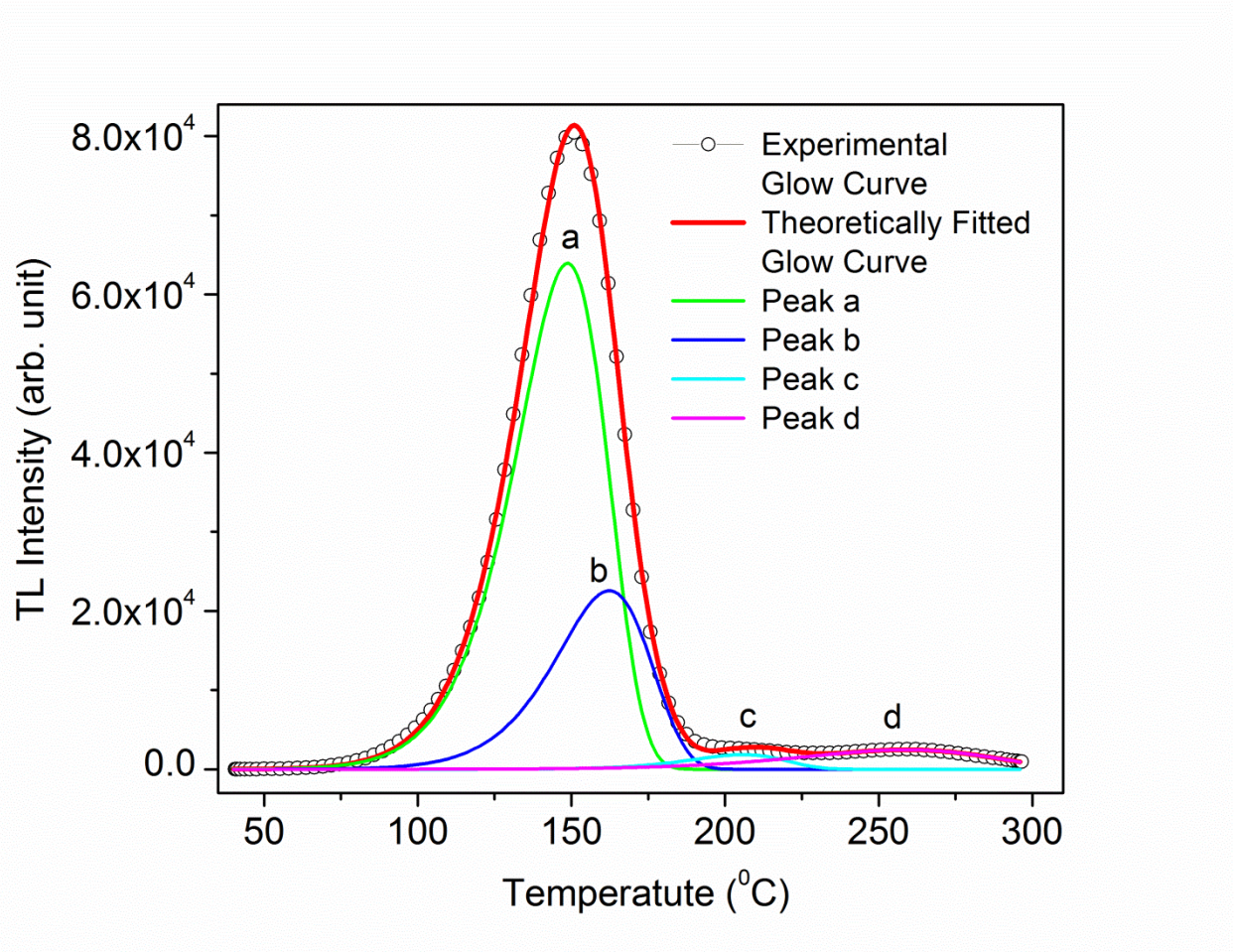
8.0x10^4
6.0x10^4
4.0x10^4
2.0x10^4
0.0
TL Intensity (arb. unit)
50
100
150
200
250
300
Temperatute (^0C)
a
b
c
d
Experimental Glow Curve
Theoretically Fitted Glow Curve
Peak a
Peak b
Peak c
Peak d

Fig. 8.

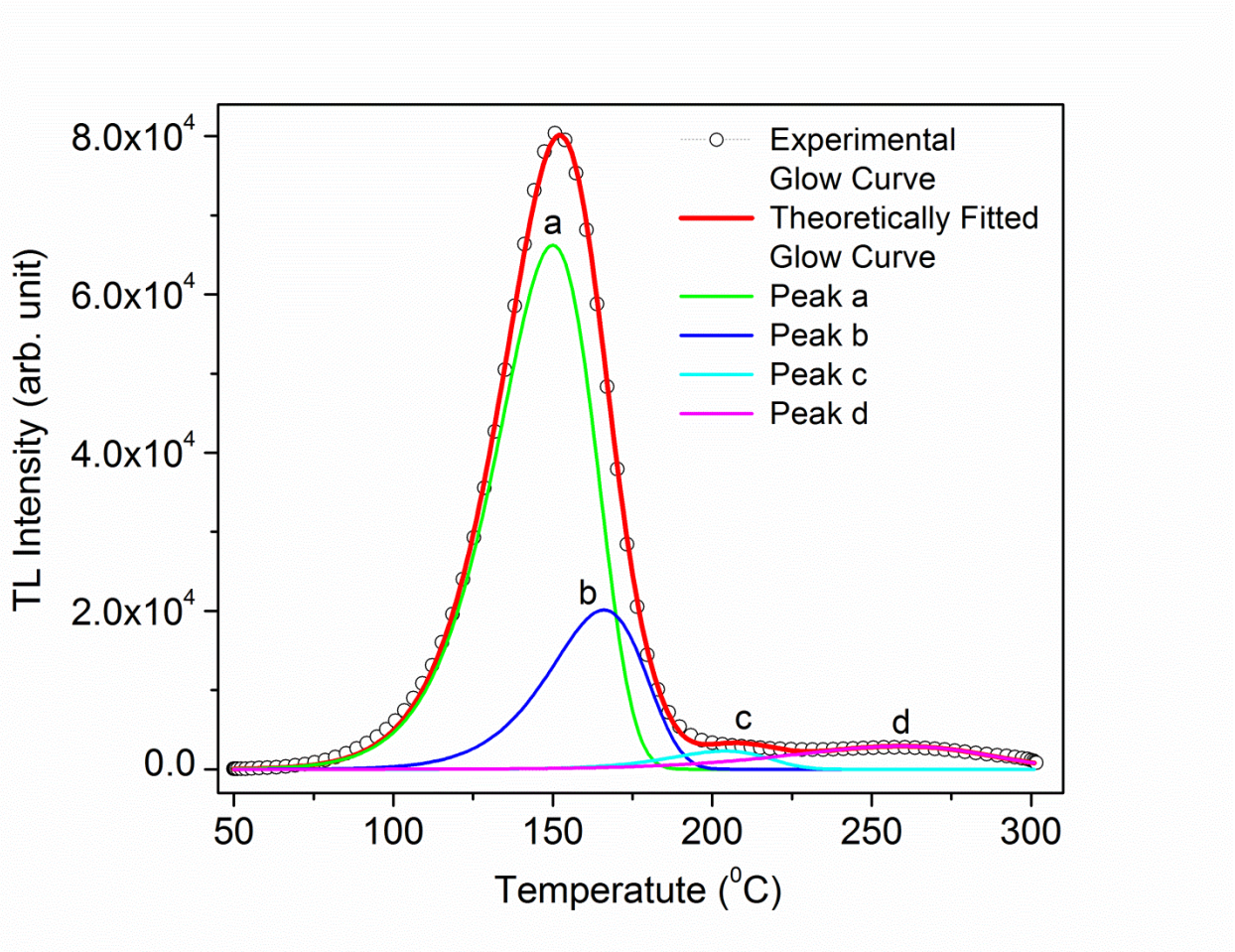
8.0x10^4
6.0x10^4
4.0x10^4
2.0x10^4
0.0
TL Intensity (arb. unit)
50
100
150
200
250
300
Temperatute (^0C)
a
b
c
d
Experimental Glow Curve
Theoretically Fitted Glow Curve
Peak a
Peak b
Peak c
Peak d

Fig. 9.

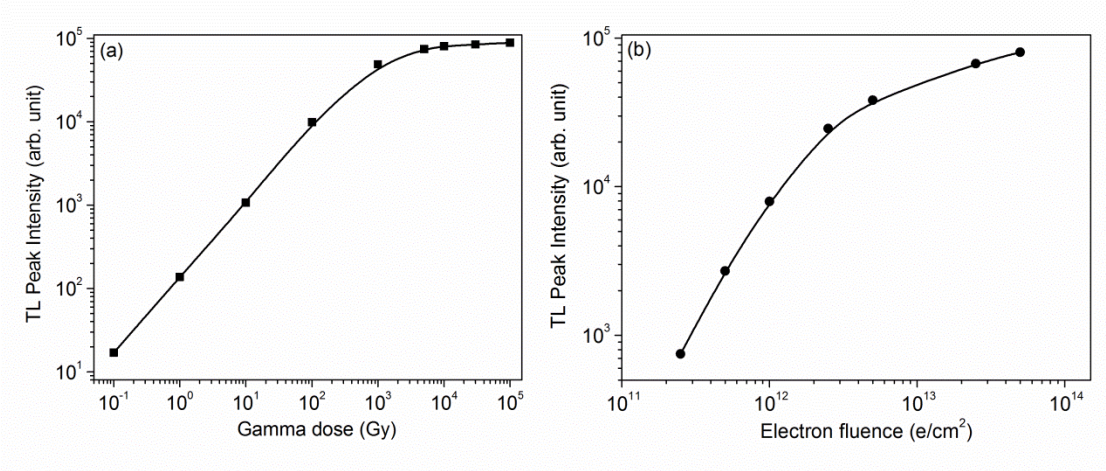
(a)
TL Peak Intensity (arb. unit)
Gamma dose (Gy)
(b)
TL Peak Intensity (arb. unit)
Electron fluence (e/cm^2)

Fig. 10.

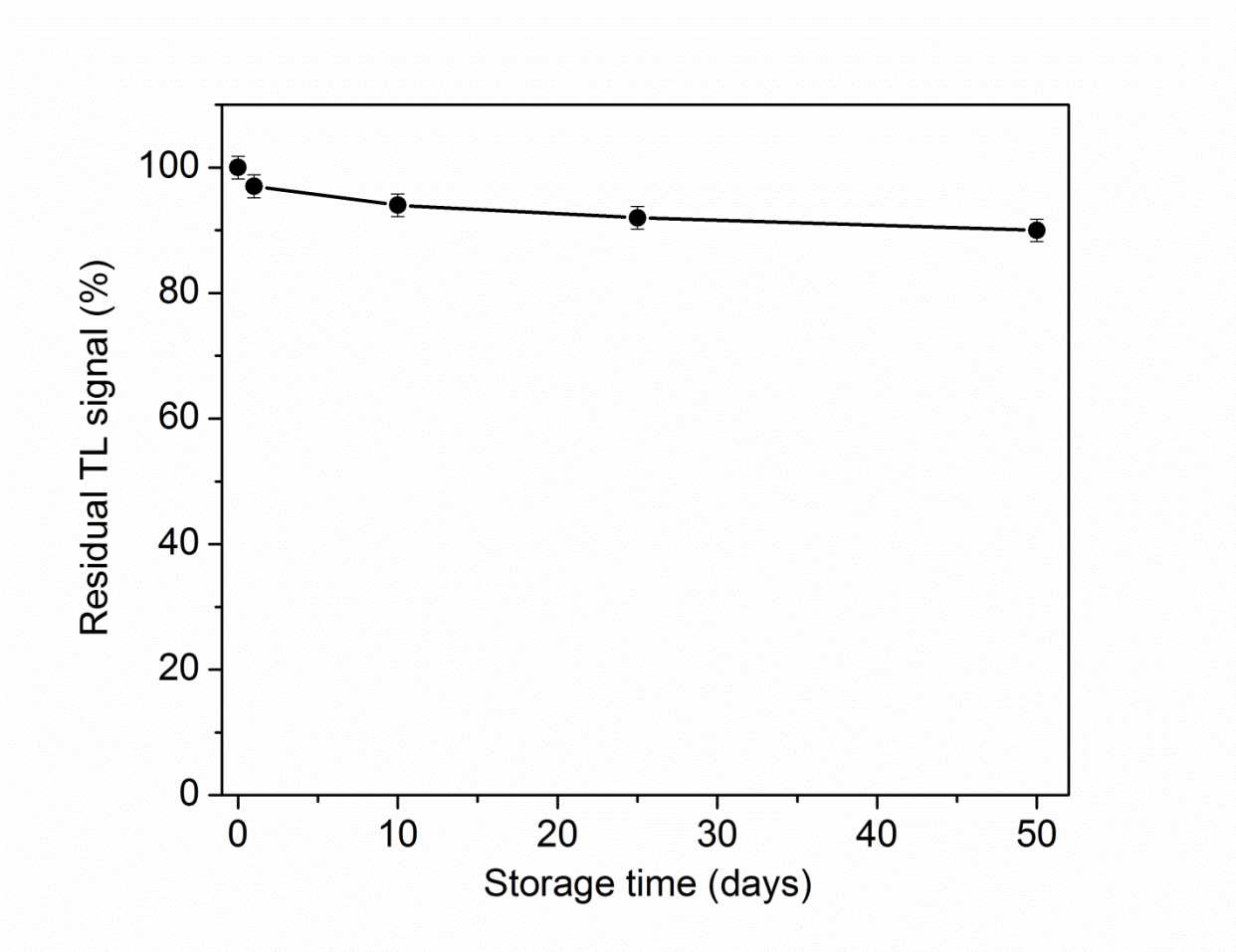
Residual TL signal (%)
100
80
60
40
20
0
0
10
20
30
40
50
Storage time (days)

Fig. 11.

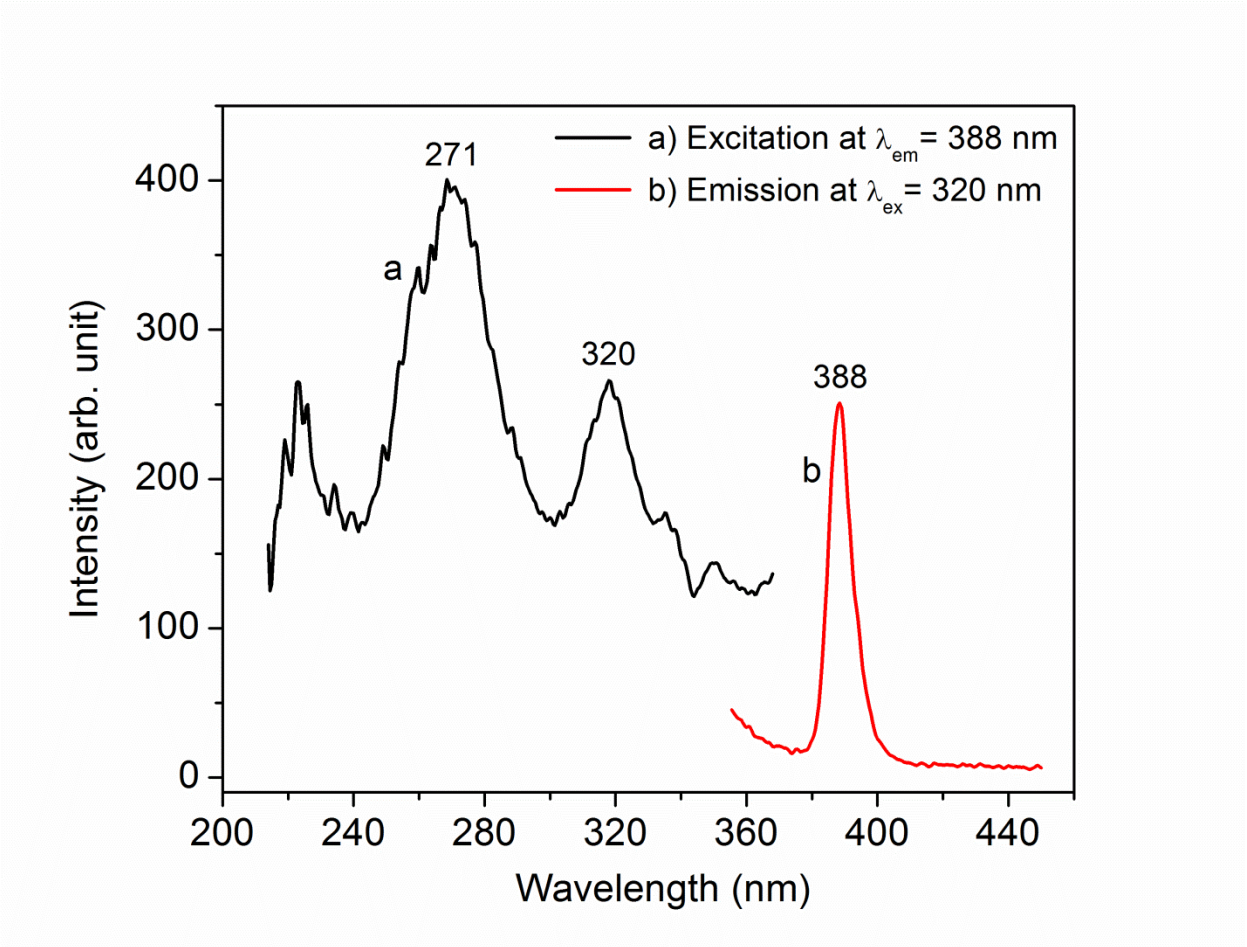
a) Excitation at λem= 388 nm
b) Emission at λex= 320 nm
271
a
320
388
b
Intensity (arb. unit)
Wavelength (nm)
0
100
200
300
400
200
240
280
320
360
400
440

Fig. 12.

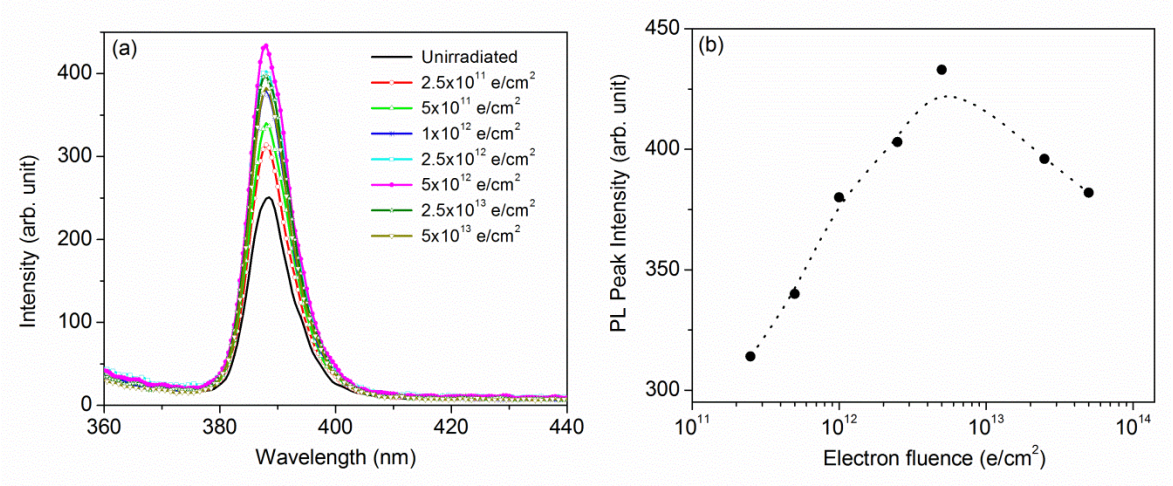
(a)
Unirradiated
2.5x10^11 e/cm^2
5x10^11 e/cm^2
1x10^12 e/cm^2
2.5x10^12 e/cm^2
5x10^12 e/cm^2
2.5x10^13 e/cm^2
5x10^13 e/cm^2
Intensity (arb. unit)
Wavelength (nm)
(b)
PL Peak Intensity (arb. unit)
Electron fluence (e/cm^2)

Fig. 13.

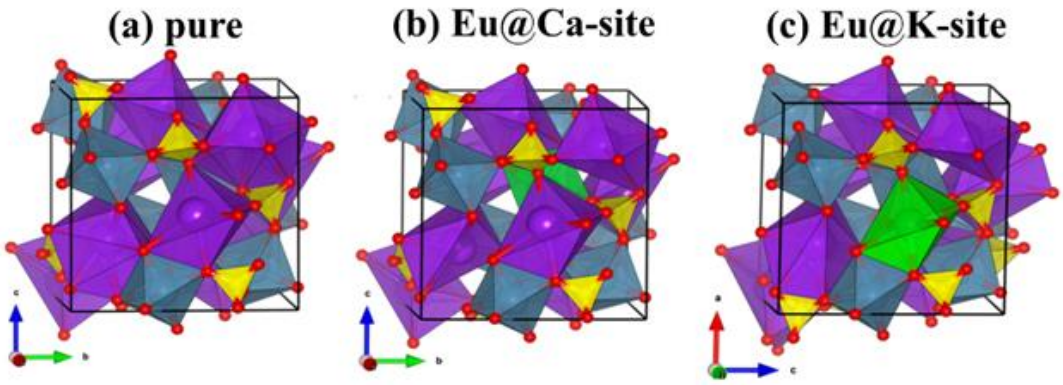

Fig. 14.

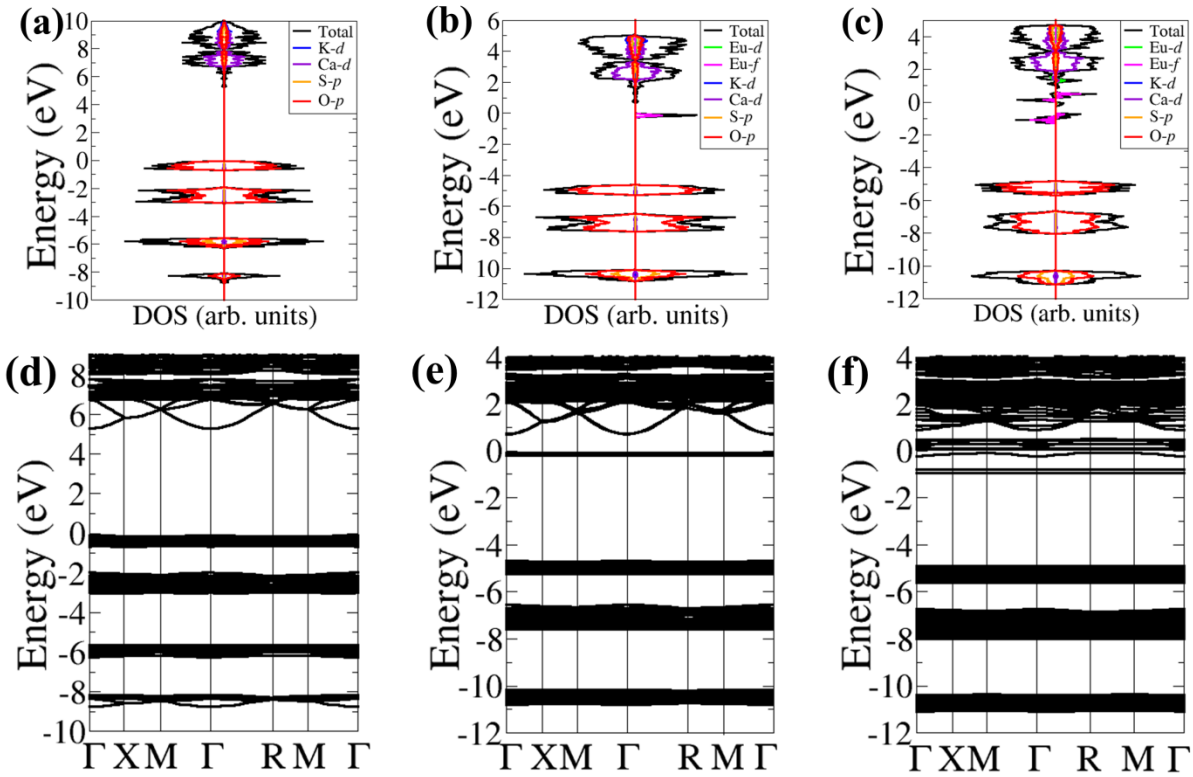

Table 1 The wt % and atomic % of the elements present in $K_2Ca_2(SO_4)_3$:Eu nanophosphor.

Elements	Atomic%	Weight% (mass%)
O	87.80	74.20
S	0.56	0.95
K	1.26	2.60
Ca	10.34	21.89
Eu	0.05	0.36
Total	100	100

Table 2: Trapping parameters of $K_2Ca_2(SO_4)_3$:Eu nanophosphor irradiated by 10 kGy gamma dose and 5×10^{13} e/cm^2 electron fluence. All the deconvoluted peaks are fitted by first order kinetics (i.e., by considering b = 1).

Irradiated with	**Peak**	**Peak Temp. T_m (°C)**	**Peak Temp. T_m (K)**	**Trap Depth E (eV)**	**Frequency factor S (s^{-1})**	**FOM**
10 kGy Gamma dose	***a***	149	422	0.9955	2.66×10^{11}	1.87%
	b	162	435	1.0282	2.73×10^{11}	
	c	206	479	1.2418	3.88×10^{12}	
	d	259	532	0.7428	1.72×10^{6}	
5×10^{13} e/cm^2 Electron Fluence	***a***	150	423	0.9726	1.29×10^{11}	1.92%
	b	166	439	1.0794	8.50×10^{11}	
	c	204	477	1.2289	3.21×10^{12}	
	d	259	532	0.7450	1.81×10^{6}	

Table 3: Electron fluences and corresponding calculated doses.

Electron fluence (n) (e/cm^2)	Dose calculated from ESTAR code (D) (Gy)
2.5×10^{11}	72.5
5×10^{11}	145
1×10^{12}	290
2.5×10^{12}	725
5×10^{12}	1450
2.5×10^{13}	7250
5×10^{13}	14500